ELSEVIER
Guide for Authors | About | Explore this Journal
REDOX BIOLOGY

Redox Biol. 2020 Sep; 36: 101557. PMCID: PMC7283154
Published online 2020 May 26. doi: 10.1016/j.redox.2020.101557 PMID: 32506037

Nox4 – RyR1 – Nox2: Regulators of micro-domain signaling in skeletal muscle

Tanya R. Cully and George G. Rodney*

Department of Molecular Physiology and Biophysics, Baylor College of Medicine, Houston, TX, USA
George G. Rodney: rodney@bcm.edu
*Corresponding author. rodney@bcm.edu

Received 2020 Mar 11; Revised 2020 Apr 10; Accepted 2020 Apr 23.

Abstract

The ability for skeletal muscle to perform optimally can be affected by the regulation of Ca^{2+} within the triadic junctional space at rest. Reactive oxygen species impact muscle performance due to changes in oxidative stress, damage and redox regulation of signaling cascades. The interplay between ROS and Ca^{2+} signaling at the triad of skeletal muscle is therefore important to understand as it can impact the performance of healthy and diseased muscle. Here, we aimed to examine how changes in Ca^{2+} and redox signaling within the junctional space micro-domain of the mouse skeletal muscle fibre alters the homeostasis of these complexes. The dystrophic *mdx* mouse model displays increased RyR1 Ca^{2+} leak and increased NAD(P)H Oxidase 2 ROS. These alterations make the *mdx* mouse an ideal model for understanding how ROS and Ca^{2+} handling impact each other. We hypothesised that elevated t-tubular Nox2 ROS increases RyR1 Ca^{2+} leak contributing to an increase in cytoplasmic Ca^{2+}, which could then initiate protein degradation and impaired cellular functions such as autophagy and ER stress. We found that inhibiting Nox2 ROS did not decrease RyR1 Ca^{2+} leak observed in dystrophin-deficient skeletal muscle. Intriguingly, another NAD(P)H isoform, Nox4, is upregulated in mice unable to produce Nox2 ROS and when inhibited reduced RyR1 Ca^{2+} leak. Our findings support a model in which Nox4 ROS induces RyR1 Ca^{2+} leak and the increased junctional space [Ca^{2+}] exacerbates Nox2 ROS; with the cumulative effect of disruption of downstream cellular processes that would ultimately contribute to reduced muscle or cellular performance.

Keywords: Skeletal muscle, Calcium, NAD(P)H oxidase, Nox2, Nox4, Dystrophy, RyR1, DMD, *Mdx*

Graphical abstract

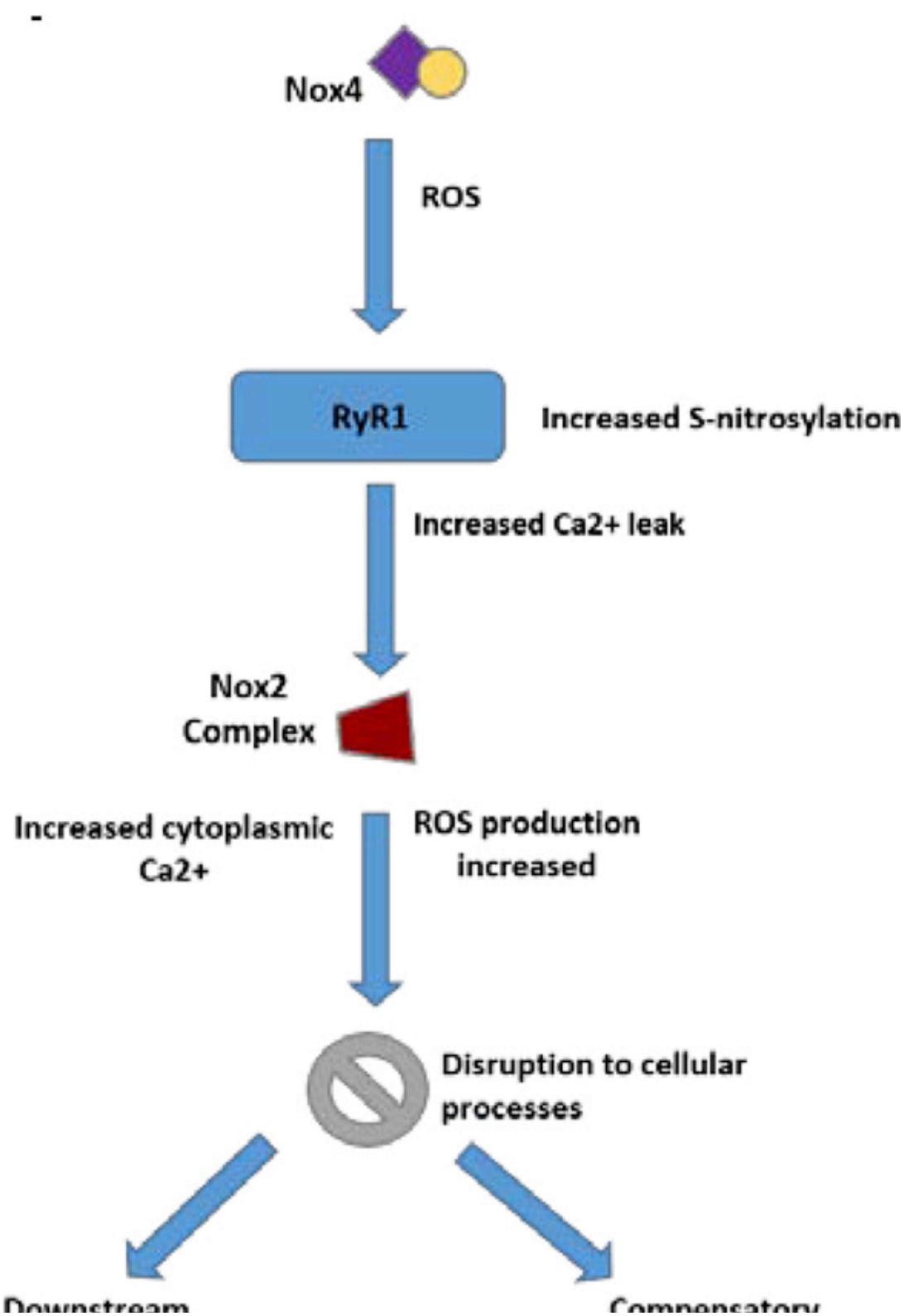

Open in a separate window

Abbreviations

Ca^{2+} Calcium
Cyto Cytoplasmic
DMD – Duchenne Muscular Dystrophy
Nox – Nicotinamide adenine dinucleotide phosphate oxidase
ROS – reactive oxygen species
RyR1 – Ryanodine Receptor one

1. Introduction

In skeletal muscle, Ca^{2+} release from the sarcoplasmic reticulum (SR), or Ca^{2+} store, to the contractile apparatus during excitation-contraction coupling (EC coupling) is tightly regulated [1]. Action potentials propagate down the plasma membrane into the tubular (t-) system to stimulate intracellular Ca^{2+} release channels/ryanodine receptors (RyR1) on the terminal cisternae of the SR. The t-system and SR terminal cisternae are closely apposed; these junctional membranes form a highly specialised nano-environment that is essential to the regulation of ion levels in the muscle fibre [[2], [3], [4]]. Impaired ability of the muscle to respond to action potentials could be the result of Ca^{2+} mishandling and oxidative stress when the fibre is at rest.

Muscle weakness in myopathies can be due to changes in the ryanodine receptor (RyR1) function resulting from a direct RyR1 genetic mutation or other modifications that have a consequential impact on the RyR1. These changes can cause muscle weakness by reducing the amount of Ca^{2+} released following excitation and by activating Ca^{2+}-dependent signaling cascades (i.e. proteases and redox signaling) in the cytoplasm [[5], [6], [7]].

NAD(P)H oxidases (Nox) are significant contributors to a cell's overall redox state [8,9]. Once thought to only be present in phagocytic cells, Nox isoforms have been identified in a variety of cell types and found to have specific functions based on the environment in which they are located [8,9]. Skeletal muscle is known to contain two of the Nox isoforms, Nox2 and Nox4. The canonical Nox2 complex consists of membrane-bound gp91 phox and p22 phox subunits and cytosolic subunits p67, p40 and p47 phox [[8], [9], [10]]. For Nox2 derived reactive oxygen species (ROS) production, all of the subunits must come together. However, in mouse models where the subunit p47 phox is rendered inactive, Nox2 ROS is unable to be produced [[11], [12], [13], [14]]. Nox4, whose biological role in skeletal muscle is not well known [9], is believed to act as an oxygen sensor [15,16]. Unlike other Nox isoforms, Nox4 is constitutively active and has one membrane-bound subunit, p22 phox [9,16,17]. In striated muscle, Nox4 is located at the surface membrane as well as at the SR [9,15]. Within the SR it has been identified to be predominantly expressed at the terminal cisternae [15]. Interestingly, Nox4 has been suggested to affect RyR1 function, potentially via nitrosylation [15]. Given the close association of Nox4 to the RyR1, Nox4 ROS could alter RyR1 function; however, a clear link has yet to be established.

Reactive oxygen species; specifically NAD(P)H oxidases located on the t-tubule are suggested to have a role in many muscle diseases with early pathological involvement in inflammation, decreased muscle function and alterations in Ca^{2+} handling [13,[18], [19], [20]]. Lack of a membrane stabilisation protein, dystrophin, can cause an initial stage of muscle degeneration induced by a disruption of Ca^{2+} regulation in the muscle [[21], [22], [23], [24]]. The *mdx* mouse, a model of dystrophin deficiency and muscle pathology, is known to have deregulated Ca^{2+} handling and harmful levels of ROS production [21,[23], [24], [25], [26], [27], [28], [29], [30]]. In addition, RyR1 displays an enhanced Ca^{2+} leak due to hyper-nitrosylation [31,32]. This model provides an ideal platform for examining the interplay

between Ca^{2+} and ROS within a cellular micro-domain. How ROS can affect Ca^{2+} signaling and how Ca^{2+} can also then propagate ROS in a reciprocal manner is slowly becoming clear; however, there is still a paucity of knowledge as to functional consequences [19,22,24,25].

Here we describe ROS and Ca^{2+} interactions within the triadic cleft micro-domain of skeletal muscle. We show that the commonly examined t-tubular Nox2 ROS does not promote RyR1 leak; instead, Nox2 ROS production is likely exacerbated by Ca^{2+} leak in the junctional cleft. For the first time, we show that Nox4 has increased expression in skeletal muscle that is unable to produce Nox2 ROS. We also show that pharmacological and genetic inhibition of Nox4 reduced RyR1 Ca^{2+} leak and that $Nox4^{-/-}$ skeletal muscle displays less nitrosylation of the RyR1 compared to WT. Our data suggest that Nox4 dependent nitrosylation of RyR1 exacerbates SR Ca^{2+} leak.

2. Materials and methods

2.1. Animal models

WT (C57BL/6J, Stock No:000664), *mdx* (C57BL/10ScSn-*Dmd*^{mdx}/J, Stock No:001801), $p47^{-/-}$ (B6(Cg)-Ncf1m1/J, Stock No:004742) and $Nox4^{-/-}$ (B6.129-Nox4tm1Kkr/J, Stock No:022,996) mice were purchased from JAX and maintained in colonies. $p47^{-/-}$ mice were generated via the insertion of a neo cassette that interrupts exon 7, the exon known for gene function [14]. The interruption of exon 7 results in a non-functional p47 phox protein, yet the protein remains detectable. The $Nox4^{-/-}$ mouse was generated using a neo cassette that replaces exon 4 within the Nox4 gene, resulting in a loss of Nox4 gene and protein expression [33,34]. Creation of the $p47^{-/-}$/*mdx* mice has been described previously [13].

2.2. Muscle preparation for single EDL fibre imaging

All experimental methods using rodents were approved by IACUC at Baylor College of Medicine. Male mice at 4 – 6weeks of age were euthanised via isoflurane overdose and cervical dislocation. The extensor digitorum longus (EDL) muscle were rapidly excised from the animals and placed in a Petri dish under paraffin oil above a layer of Sylgard. Rhod-5N salt was trapped in the sealed t-system as originally described by Lamb et al. (1995) [35]. Briefly, small bundles of fibres were isolated using fine forceps and exposed to a Na^+-based physiological solution (external solution) containing (mM): Rhod 5 N 2.5, $CaCl_2$, 2.5; NaCl, 132; $MgCl_2$, 1; KCl, 3.3; HEPES, 20 and the pH was adjusted to 7.4 with NaOH. The dye was allowed more than 10 min to diffuse into the t-system from the surrounding bubble of solution containing fluorescent dye. After this equilibration period, individual fibres that had been exposed to the dye solution were isolated from the bundle and mechanically skinned. After skinning, the fibre was transferred to an experimental chamber containing a K^+-based internal solution which allowed the sealed t-system to generate a normal resting membrane potential (Lamb & Stephenson, 1990[36]; 1994[37]). The solution contained (mM): Mg^{2+},1 (added as MgO); HDTA, 49; EGTA, 1; HEPES, 10; K^+, 103–106 (added as KOH); Na^+, 36 (from ATP and CP); ATP, 8; creatine phosphate, 10; sucrose 103–107 and N-Benzyl-p-toluenesulfonamide (BTS), 0.05 with pH adjusted (with KOH) to 7.1.

2.3. RyR1 Ca^{2+} leak measurements

Under resting control conditions Ca^{2+} leaks from the RyR1 and is extruded from the intracellular junctional space to the extracellular environment via the plasma membrane Ca^{2+} ATPase (PMCA) and the Sodium/Ca^{2+} exchanger (NCX) (Fig. S1A). Tetracaine is used to inhibit the RyR1 in order to prevent the local leak of Ca^{2+} into the diffusionally restricted junctional space [3,31]. Subsequently, the

uptake of Ca^{2+} by PMCA and NCX corresponds to diffusion of Ca^{2+} from the bulk cytoplasm and not from the RyR1 leak (Fig. S1B). Any separation between the control and tetracaine curves (Fig. 1D–F) is an indication of RyR1 Ca^{2+} leak.

Open in a separate window

Fig. 1

T-system Ca^{2+}measurements show presence of a large RyR leak in *mdx*,p47$^{-/-}$/*mdx and* p47$^{-/-}$mice.. **A,B,** Representative trace of WT and *mdx* mice t-sys uptake at 200 nM $[Ca^{2+}]_{cyto}$ with and without tetracaine. Vertical grey bars indicate solution exchange artifacts during confocal acquisition. **C-F,**Steady-state $[Ca^{2+}]$t-sys was determined for a broad range of resting $[Ca^{2+}]_{cyto}$ (28–1300 nM) in age-matched mice; separation in the two curves (with and without tetracaine) is due to RyR Ca^{2+} leak (see Methods Fig. S1). Closed circles represent control, open circles with the addition of 1 mM tetracaine.

2.4. Confocal imaging

Mounted skinned fibres were imaged using a Zeiss 780 inverted confocal microscope equipped with a Zeiss 1.2NA 40× Plan-Apochromat water immersion objective. Rhod-5N was excited with a 561 nm laser diode. For tracking Ca^{2+} movements across the t-system membrane, images were continuously recorded in xyt mode with an aspect ratio of 512 × 256, with the long aspect of the image parallel with that of the fibre. Temporal resolution of imaging in this mode where the fluorescence signal was measured from within the borders of the fibre was 0.3 s/frame.

2.5. Image analysis for Ca^{2+} measurements

t-system (t) rhod-5N fluorescence (F (t)) was collected by continuous xyt imaging during multiple internal solution changes. At the end of the experiment each fibre was exposed to ionophore (20 μM) and 5 mM Ca^{2+}, followed by 0 Ca^{2+} to obtain the fluorescence maximum (Fmax) and minimum (Fmin), respectively. These values were used in conjunction with the previously determined K_D of Rhod-5N in the t-system of 0.8 mM [[3], [38], [39]] to determine $[Ca^{2+}]_{t\text{-}sys}$, with the relationship: $[Ca^{2+}]_{t\text{-}sys}$ (t) = $k_{D,Ca}$ * (F (t) – Fmin)/(Fmax – F (t)).

2.6. Western blotting

A whole muscle homogenate was prepared using flash-frozen EDLs as described by Murphy et al. 2006 [6]. Briefly, muscle (8–12 mg), was weighed and homogenised on ice (1:20 w/v) in a K-EGTA solution containing (mM):103 K^+ (from KOH), 50 EGTA, 90 HEPES, 1 Mg^{2+} (from MgO), 8 total ATP, 10 creatine phosphate, pH 7.10) with a protease inhibitor cocktail (PIC, Complete; Roche). Immediately following this, the homogenate was diluted to 1:50 with the K-EGTA and PIC solution and then 1:1 with 2x SDS Laemmli buffer. A small amount of homogenate from all samples was mixed to generate a suitable sample for 4 point calibration curves, spanning 3–60 μg of total muscle wet weight [[40], [41], [42], [43], [44]]. Samples were electrophoresed for 30 min at 200 V using 4–15% or 10% stain free tris/glycine gels and transferred overnight at 4 °C and 30 V. PVDF membranes (BioRad) were blocked in 5% skim milk in TBST or 3% BSA in PBST; primary antibodies were probed in 1% BSA in PBST. Chemiluminescent images were acquired on a BioRad Chemidoc Touch using BioRad Clarity and Clarity Max ECL reagents. Images were analysed using BioRad Image lab software.

Stain-free tris/glycine gels (BioRad) were utilised in order to assess total protein loading and normalisation for Western blot analysis. The use of stain-free total protein technology reduces the possibility of genotype and age-dependent changes of housekeeping proteins such as GAPDH and actin [[40], [41], [42], [43], [44], [45], [46], [47], [48], [49]]. Western blot figures are displayed with protein of interest representative blots and myosin heavy chain (MHC) as a visual indicator of protein loaded. Analysis utilised total protein from the stain-free gels.

For studies analysing the RyR1, 4–12% bis/tris gels were utilised. These gels were not stain-free and were post-stained with Coomassie blue for myosin heavy chain (MHC) density. Total RyR1 was then normalized to MHC for protein loading differences. See Supplementary Materials Fig. 2.

Open in a separate window

Fig. 2

Western blotting of WT, *mdx*, p47$^{-/-}$, p47$^{-/-}$/*mdx*and Nox4$^{-/-}$ EDL total protein lysates for Nox4 and p22 phox subunit. A.We found that Nox4 protein expression was increased in mice that lack p47 phox. As Nox4 is constitutively active an increase in Nox4 protein would likely indicate increased ROS production.**B**, The p22 subunit is required for both Nox2 and Nox4 ROS production. p22 was found to be significantly increased in muscle that lacked the expression of dystrophin **C,** Nox2 expression levels in WT, p47$^{-/-}$and Nox4$^{-/-}$. **D,** p47 phoxprotein levels in WT, p47$^{-/-}$and Nox4$^{-/-}$, N·B.the p47$^{-/-}$is a misnomer, the mouse still has p47 phox protein but it is inactive. **E,** p47 phox pSer370 expression is unchanged in Nox2 and Nox4 ROS deficient mice. **F,** Ratio of p47 phox pSer370 to p47 phox total, no change in all genotypes. * denotes significantly different to WT $p < 0.05$, ** indicates $p < 0.01$, ***$p < 0.001$, ****$p < 0.0001$.

2.7. Antibodies

Antibodies used in this paper and the working concentrations are provided in Supplementary Table 1.

2.8. S-Nitrosylation biotin switch assay

Whole muscle, EDL lysates were processed via the biotin switch method using the S-nitrosylated Protein Detection Kit (Cayman Chemical). Biotin switch samples were run on a 4–12% Bis-Tris gel and transferred to PVDF. The membrane was blocked in 3% BSA in PBS-Tween, and the secondary HRP was used to detect total nitrosylation. The membrane was then stripped and re-probed for RyR1 total protein levels. The nitrosylation of the band at the MW of RyR1 was then expressed relative to the total RyR1 protein density in the sample.

2.9. Carbonylation assay

Whole muscle EDL lysates were derivatized according to the manufacturer's directions in order to determine levels of carbonylation (EMD Millipore, Oxyblot Kit). After derivatization and neutralization, samples were run on a 4–12% Bis-Tris gel and transferred to PVDF overnight. The membranes were blocked in 1% BSA in PBS-Tween and probed using anti-DNP and secondary antibodies provided in the kit. For analysis of total sample carbonylation whole lanes were used and expressed relative to total protein (MHC).

2.10. Force measurement

EDL muscles were dissected, placed in a physiological saline solution containing (mM): NaCl 120, KCl 4, CaCl 2, $MgSO_4$ 1, $KH2PO_4$ 1, $NaHCO_3$ 25, glucose 10 and continuously gassed with 95% O_2–5% CO_2. Muscle length and voltage were adjusted to elicit maximum twitch force. Force-frequency characteristics were measured at 1, 5, 10, 20, 40, 80, 120, 150, 200 and 300 Hz every 1 min. Fatigue was performed at 70 Hz tetani for 5 min, followed by a recovery protocol consisting of a 30 Hz and 100 Hz tetani every minute for 10 min. At the end of the contractile protocol, muscle length and weight were determined to assess absolute forces expressed as N/cm [2].

2.11. Isolation of single, intact enzymatically dissociated FDB fibres

Flexor digitorum brevis (FDB) muscles were placed in a dish containing DMEM media supplemented with 1% penicillin/streptomycin (Gibco) and 4 mg/ml of collagenase (Sigma). After 1 – 2 hrs at 37 °C, the muscles were triturated with decreasing bore sizes of fire-polished pipettes to yield single fibres. Cultures were maintained at 37 °C in DMEM with 1 % pen/strep and 10% FBS for a maximum of 48 h s.

2.12. DCF ROS measurements:

Intact FDB fibres were plated on 96 well plates using ECM (Sigma). Fibres were loaded with 5 μM DCFH-DA (Molecular Probes) at 37 °C. After de-esterification fibres were imaged on a Sutter Lamda DG-4 Ultra-high-speed wavelength switcher was used to excite DCF (480 nm) emission intensity was collected at 510 nm on a charge-coupled device (CCD) Camera (CoolSNAP MYO, Photometrics) attached to an Axio Observer (Zeiss) inverted microscope at 0.1 Hz. Baseline measurements were collected for 50 s and maximal oxidation elicited via the addition of 1 mM H_2O_2 at the end of imaging. Linear curves were fitted to the data at 15–40 s of baseline and the final 40 s of maximal response to H_2O_2 to calculate the slopes. The values of the slopes were then used to create a ratio of base over max in order to determine the oxidative state of the fibre.

2.13. Statistical analysis

Data is presented as mean ± SEM. A one-way ANOVA was performed for statistical analysis with Dunnetts post-hoc multiple comparisons to WT control unless otherwise stated. Statistical analysis was performed with Graph Pad Prism.

3. Results

3.1. Genetic inhibition of Nox2 ROS does not abolish RyR1 leak in *mdx* or WT mice

For initial experiments, we utilised the *mdx* mouse due to the perturbations in Ca^{2+} and ROS handling presented in this model. Use of the dystrophin-deficient mouse allowed us to assess micro-domain Ca^{2+} regulation in the presence or absence of different Nox isoforms in order to investigate the influence of redox changes on the RyR1.

Mdx mice are reported to have RyR1 Ca^{2+} leak at the pathologically critical degeneration/regeneration timepoint [31,32]. In Fig. 1A–D, we show the presence of RyR1 Ca^{2+} leak in the early period of the dystrophic *mdx* mouse where the muscle undergoes cycles of degeneration and regeneration; this leak was consistent with previous reporting [32]. We wished to examine the level of RyR1 leak in dystrophic mice that could not generate Nox2 ROS ($p47^{-/-}$/*mdx*); with the hypothesis that the increased level of Nox2 ROS observed in the *mdx* mouse at 19 days was contributing to leak of Ca^{2+} from the RyR1 [[19], [20], [29]]. We have previously shown that $p47^{-/-}$/*mdx* mice display improved muscle pathology and improvement in force production [13,50]. We targeted the same 4–6 week time period used in measurements of the *mdx* mouse for analysis of RyR1 Ca^{2+} leak in $p47^{-/-}$/*mdx* mice. A

pronounced RyR1 leak was present in both p47$^{-/-}$/*mdx* (Fig. 1E), and in dystrophin positive p47$^{-/-}$ control mice (Fig. 1F) despite the improvement in pathology previously reported in this model [13,50,51].To pharmacologically block Nox2 ROS production, we applied the gp91ds peptide during RyR1 leak experiments in WT, *mdx* and p47$^{-/-}$ mice. We observed a non-specific inhibition of the RyR1 with the peptide (data not shown), rendering it inappropriate for use in our skinned fibre studies.

3.2. Eliminating Nox2 ROS elevates Nox4 protein levels

EDL whole muscle homogenates from WT, *mdx*, p47$^{-/-}$ and p47$^{-/-}$/*mdx* were probed via Western blot to determine the expression levels of redox proteins Nox4 and p22 phox. In p47$^{-/-}$ and p47$^{-/-}$/*mdx* mice, which are unable to produce Nox2 ROS, Nox4 expression increased significantly ($p = 0.001$) (Fig. 2A). Nox4 has been suggested to be constitutively active with its only other accessory subunit being p22 phox [15,17,52]. Therefore, for higher amounts of Nox4 ROS production, increased Nox4 expression is necessary [53]. *Mdx* and p47$^{-/-}$/*mdx* mice were found to have significantly increased p22 phox levels compared to WT (Fig. 2B). The increase in p22 phox in *mdx* mice is inconsistent with previous reporting [29]; however in our circumstances whole, non-fractionated tissue homogenate was used, and mice were at least ten days older.

To examine if elimination of Nox4 induced a reciprocal increase in Nox2 complex proteins, p47 phox and Nox2 expression levels were examined in Nox4$^{-/-}$ EDL lysates. No change was present in the expression levels of p47 phox or Nox2 in the Nox4 ROS deficient animals (Fig. 2C-D). However, this does not necessarily indicate that there would be no change in the ROS producing activity of these proteins. Note that the presence of p47 phox protein in the p47$^{-/-}$ is due to the manner the mouse was created, there is protein present but it is not active. The phosphorylation levels of a specific phosphoserine site, pSer370 on p47 phox were assessed via western blotting. Expression of p47 phox pSer370 in the Nox4$^{-/-}$ mice was not increased compared to WT, suggesting that p47 phox activity is not increased (Fig. 2F).

The presence of RyR1 Ca^{2+} leak in the dystrophin positive p47$^{-/-}$ control mice in addition to the elevation of Nox4 expression, provided an intriguing and unexpected avenue for subsequent studies on triadic cleft micro-domain signaling independent of dystrophin deficiency.

3.3. Basal ROS production is no different in Nox4 ROS deficient mice

Basal redox state was assessed in WT and Nox4$^{-/-}$ deficient mice using DCFH-DA in intact FDB fibres. Fig. 3A shows a representative trace of DCF fluorescent activity in WT and Nox4$^{-/-}$ mice. The ratio of base slope over max slope was calculated as an indication of the oxidative capacity of the individual fibres (Fig. 3B). No significant difference was found ($p = 0.497$, nested *t*-test) in the basal oxidative capacity of the Nox4 ROS deficient mice suggesting a similar redox state within the bulk cytoplasm to that of WT.

Open in a separate window

Fig. 3

Basal redox state was assessed in WT and Nox4$^{-/-}$deficient mice using DCFH-DA in enzymatically isolated intact FDB fibres. A. A representative trace of DCF fluorescent activity in WT and Nox4$^{-/-}$mice. Linear curves were fit to the data with lines indicated in green showing slopes fit to the baseline data (15–40s), lines in red display slopes fit to the maximum response of the curve (80–120s). **B.**The ratio of base slope over max slope was calculated as an indication of the oxidative capacity of the respective fibres. No significant difference ($p = 0.497$, nested *t*-test) was found in the basal oxidative capacity of the Nox4 ROS deficient mice suggesting a similar redox state to that of WT. (For interpretation of the references to colour in this figure legend, the reader is referred to the Web version of this article.)

Nox4 deficient mice displayed no changes in force production or fatigue recovery. Force frequency, fatigue and recovery from fatigue were assessed in 4–6 week old C57Bl6 WT mice and Nox4 deficient mice. Recovery was performed at 30 Hz and 100 Hz to observe potential effects on low-frequency recovery due to ROS [54]. No change in specific force was observed or any alteration in the rate of fatigue or recovery (Fig. S3). Of note, both genotypes did not recover force at 30 Hz to the degree seen at 100 Hz.

3.4. Calcium handling proteins are not altered in Nox 4 ROS deficient muscle

To examine the potential interplay between calcium flux and ROS production, we quantified the levels of critical calcium handling proteins. STIM1S, “short” isoform of STIM1, is an SR calcium sensor involved in the process of store-operated calcium entry (SOCE) which has previously been shown to be upregulated in the *mdx* mouse at 3 months of age [27]. SOCE can locally raise Ca^{2+} levels in the junctional space and the cytoplasm in response to SR Ca^{2+} reduction [[55], [56], [57], [58]]. We found no statistical differences in the levels of STIM1S [59,60] in either p47$^{-/-}$, or Nox4$^{-/-}$ mice compared to WT (Fig. 4A). Interestingly, we observed a significant increase in STIM1S expression in only the p47$^{-/-}$/*mdx* mouse compared to WT ($p = 0.0073$) (Fig. S4). Calsequestrin 1, an important SR Ca^{2+} buffering protein, is not statistically different in p47$^{-/-}$, Nox4$^{-/-}$ and p47$^{-/-}$/*mdx* mice at 4 weeks of age (Fig. 4B). In addition, the Sarco/endoplasmic reticulum ATPase 1 (SERCA1), responsible for the uptake of Ca^{2+} from the cytoplasm to the SR, is not different in p47$^{-/-}$, Nox4$^{-/-}$ and p47$^{-/-}$/*mdx* mice (Fig. 4C). Therefore an increase in the uptake rate by the SERCA pump is unlikely.

Open in a separate window

Fig. 4

Calcium handling proteins, STIM1S, calsequestrin1 and SERCA 1 are not altered in Nox2 and Nox4 ROS deficient EDL muscle. A, STIM1S was found to not be different to WT in the $p47^{-/-}$ ($p = 0.08$) and $Nox4^{-/-}$ ($p = 0.8$). **B,** The SR Ca^{2+} buffer CSQ1 was found to not be different in $p47^{-/-}$ ($p = 0.5$) or $Nox4^{-/-}$ ($p = 0.6$). **C,** SERCA1 was unchanged in both $p47^{-/-}$ and $Nox4^{-/-}$ ($p = 0.9$ and 0.99 respectively). Individual values for each n are represented on each graph.

3.5. RyR1 leak is reduced with pharmacological or genetic inhibition of Nox 4

In Fig. 1, RyR1 Ca^{2+} leak was present in the $p47^{-/-}$/*mdx* mouse despite a reported improvement in pathology [13,50]. Due to the increase of Nox4 expression in the Nox2 ROS deficient mice (Fig. 2) and the location of Nox4 near the RyR1 [9,15], we sought to elucidate if genetic knockout or pharmacological inhibition of Nox4 would result in a decrease of RyR1 Ca^{2+} leak. We examined RyR1 Ca^{2+} leak in 4–6 week old Nox4 male knockout mice. We found that RyR1 leak is minimal in the Nox4 knock out mice (Fig. 5A-B). Pharmacological inhibition of Nox4 with GKT137831 (150 nM, 6–10min) reduced RyR1 Ca^{2+} leak in WT and $p47^{-/-}$ muscle across all $[Ca^{2+}]_{cyto}$ (Fig. 5C-D). Taken together, our data supports a model in which Nox4 ROS promotes RyR1 leak.

Open in a separate window

Fig. 5

Lack of Nox4 ROS production via genetic knock out or pharmacological inhibition results in lessening of RyR1 leak. A, Representative trace of $Nox4^{-/-}$ RyR1 leak. **B,** RyR1 leak is not present in the $Nox4^{-/-}$ at a variety of $[Ca^{2+}]_{cyto}$. **C,D,** Nox4 ROS inhibition with GKT137831 reduces leak. N = number of animals, n = number of fibres.

3.6. S-Nitrosylation levels and RyR1 phosphorylation are altered in Nox4 ROS deficient muscle

In order to assess whether Nox4 promotes S-nitrosylation of the RyR1, we performed a biotin switch assay using a commercially available kit to assess bulk nitrosylation of the channel. Intriguingly, RyR1 total protein was found to be upregulated in $Nox4^{-/-}$ and $p47^{-/-}$/*mdx* mice ($p = 0.0001$ and 0.01 respectively) (Fig. 6A, $p47^{-/-}$/*mdx* not shown). As we used whole, non-fractionated muscle homogenates we sought to determine potential contributors to the increased RyR1 outside of skeletal muscle itself. Circulating macrophages express RyR1 [61]; therefore, we probed for CD68 as a marker of macrophage infiltration to rule out any contribution of macrophage RyR1 to the total RyR1 protein levels in the skeletal muscle. CD68 was found to not be different in the $Nox4^{-/-}$ mouse (Fig. S6).

Open in a separate window

Fig. 6

RyR1 post-translational modifications in Nox2 and Nox4 ROS deficient mice. **A,** Total RyR1 expression in WT, $p47^{-/-}$and $Nox4^{-/-}$EDL whole muscle lysates. $Nox4^{-/-}$mice display a significant increase in total RyR1 content ($p < 0.0001$). **B,**S-nitrosylation is expressed relative to the total protein content of RyR in WT, $p47^{-/-}$and $Nox4^{-/-}$mice. S-nitrosylation is increased ($p = 0.05$) in the RyR leaky $p47^{-/-}$mice and decreased in the $Nox4^{-/-}$($p = 0.02$). **C,**Phosphorylation of the RyR1 at Serine2808 is decreased in the $Nox4^{-/-}$muscle. Individual n values are displayed on the plots, * denotes significantly different to WT $p < 0.05$, ****$p < 0.0001$.

S-nitrosylation was found to be increased relative to WT ($p = 0.05$) in the $p47^{-/-}$ and decreased in the $Nox4^{-/-}$ ($p = 0.02$) (Fig. 6B). S-nitrosylation of the RyR1 was also found not to be increased in the $p47^{-/-}$/*mdx* Fig. S5C). Phosphorylation of S2808 of RyR, a site known for regulation of RyR1 Ca^{2+} leak in cardiac and skeletal muscle [62], was found to be decreased ($p = 0.04$) in the $Nox4^{-/-}$ mice (Fig. 6C).

4. Discussion

Ca^{2+} handling and signaling within any cell type is essential for normal cell function and Ca^{2+} homeostasis in both healthy and diseased tissue [63]. Reactive oxygen species are also necessary for modulating cellular functions with alterations in the balance between reactive oxygen species and reactive nitrogen species potentially causing problems within cells if scavenging of these species is insufficient [9,10,19]. In skeletal muscle disease, it has been suggested the oxidative stress from aberrant ROS production may not itself be enough to drive pathological changes but rather the interplay between ROS/RNS and Ca^{2+} handling [19,64,65]. The *mdx* mouse model of Duchenne Muscular Dystrophy displays both aberrant Ca^{2+} handling and alteration in ROS species (particularly NAD(P)H oxidases), providing a suitable model for describing how Ca^{2+} and ROS affect each other and potentially lead to pathology [13,25,28,29,50,51].

Here, we examined the roles of two NAD(P)H oxidases in contributing to RyR1 Ca^{2+} leak, with particular focus on how one isoform, Nox4, regulates RyR1 leak and thus contributes to alterations in Ca^{2+} and ROS levels within a skeletal muscle micro-domain. While this study has been carried out in skeletal muscle, the interplay between the Nox isoforms and modulation of Ca^{2+} levels is relevant for all cell types [10].

Our experiments revealed in muscle that is unable to produce Nox2 ROS, Nox4 protein is upregulated. As Nox4 is constitutively active, increased protein expression would drive increased Nox4 ROS production [53]. Previous work on ROS has found a bell-shaped curve of ROS homeostasis in the cell [66,67]; which might explain an upregulation in Nox4 ROS in response to the loss of Nox2 ROS within a cell. The Nox4 upregulation could be a compensatory mechanism to regulate the redox state within the triadic micro-domain. Nox 4 likely has a role in regulation of RyR1 leak to induce changes in other signaling cascades and also hormesis through Nrf2 [[67], [68]].

To date, measuring Nox4 ROS production has been difficult due to the location of Nox4 in subcellular compartments [9]. Indeed, when we examined basal ROS levels in Nox4$^{-/-}$ mice using DCF, we were unable to establish differences to that of WT. This data suggests that when Nox4 ROS is eliminated that Nox2 ROS production does not increase, contrary to increased Nox4 expression that was seen in Nox2 ROS deficient p47$^{-/-}$ mice. Chemical ROS probes like DCF only allow for assessment of bulk production of ROS within the cell. Much like when measuring cytoplasmic Ca^{2+}, bulk measurements in the cytoplasm are unable to discern, or are obscuring, changes in and around cellular micro-domains. While the a genetically encoded biosensor, p47-roGFP, can detect Nox2-dependent ROS it also can induce Nox activation [69]. These imaging limitations highlight the rising usefulness of developing new genetically targeted encoded ROS and Ca^{2+} biosensors that can be targeted to micro-domains within the cell [[69], [70], [71]].

Our results showed that in dystrophic muscle and dystrophic muscle that was unable to produce Nox2 ROS, p22 phox, a subunit required for both Nox2 and Nox4 ROS production was upregulated. The upregulation of p22 phox in dystrophic tissue could be associated with the increase in p47 phox and Nox2 ROS seen in that model [13,18]. As p22 phox is membrane-embedded, the membrane disturbances associated with dystrophic tissue could also play a role in driving increased expression. It is of interest that p22 phox is a critical subunit for both Nox2 and Nox4 ROS, with different regions of the protein associating with each isoform to drive ROS production [17]. The upregulation of Nox4 in Nox2 ROS deficient muscle could be a by-product of the upregulation of p22 phox [72].

The RyR possesses thiol groups of cysteine (Cys) residues that can be affected by reactive oxygen or nitrogen species (ROS/RNS) [20,[73], [74], [75], [76]]. Both RyR1 and RyR2 have nitric oxide (NO) bound to cysteines which enables a post-translational modification (s-nitrosylation) to occur [77,78]. These post-tranlational protein modifications (s-nitrosylation, phosphorylation, glutathionylation, and alkylation) can lead to changes in the redox state of the RyR, leading to increased open or closed state of the channel, thus altering the function. Certain cysteines, such as Cys3635, have been identified to be more prone to nitrosylation modifications; with Cys3635 being redox-sensitive under physiological oxygen tension and nitrosylated to aid in muscle contraction [75,76,78].

We show that S-Nitrosylation of the RyR is reduced in the Nox4$^{-/-}$ compared to WT and modestly increased in the p47$^{-/-}$ mouse. The decrease in nitrosylation of the RyR1 in the Nox4$^{-/-}$ suggests that Nox4 ROS influences Ca^{2+} leak through the RyR1. Our measurements of RyR1 leak in the Nox4$^{-/-}$ mouse showed minimal RyR1 leak in this model. The p47$^{-/-}$ mouse showed increased Nox4 protein expression, an increase in nitrosylation of RyR1, and a corresponding increase of RyR1 leak. We also used GKT137831 as an inhibitor of Nox4 in all of our experimental mouse models; WT, *mdx*, p47$^{-/-}$, p47$^{-/-}$/*mdx*. We found that RyR1 leak was reduced in *mdx*, p47$^{-/-}$, p47$^{-/-}$/*mdx* with the Nox4 inhibitor (Fig. 5, Fig. S7). Reducing thiols with DTT (10 mM, 6 min) reduced RyR1 leak at 200 nM Ca^{2+} in the p47$^{-/-}$/*mdx* mouse model (Fig. S5D). Dutka et al., 2017 [79] have previously shown that DTT treatment of individual skinned muscle fibres resulted in the removal of S-Nitrosylation of troponin I and reduced Ca^{2+} sensitivity of the protein. In our experiment the p47$^{-/-}$/*mdx* is unable to produce Nox2 ROS, limiting the likely ROS source present to Nox4. Carbonylation experiments (Fig. S5A) also showed that whilst the p47$^{-/-}$/*mdx* mouse had reduced oxidation relative to the mdx mouse, carbonylation was still increased relative to the WT. We would suggest that the DTT is further reducing the oxidation of the p47$^{-/-}$/*mdx* muscle and potentially also removing any S-Nitrosylation modifications. The net result of both actions being that leak is heavily reduced in this mouse model.

The Marks lab has previously shown that PKA phosphorylation of the RyR at Serine2808 results in altered modulation of the RyR1 in skeletal muscle during heart failure [62,80]. Changes in phosphorylation of the RyR have also been shown in response to exercise-induced SR Ca^{2+} leak during

training [81] and cold acclimatisation [82]. We also examined the level of phosphorylation of the RyR1 at Serine2808 and found a reduction in the phosphorylation of the RyR in skeletal muscle from the Nox4$^{-/-}$ mouse. Conversely, we did not observe an increase in phosphorylation of the RyR1 in the p47$^{-/-}$, a mouse model with leak present. Comparing the phosphorylation data to the changes observed in the nitrosylation status of the RyR1, we would suggest that the nitrosylation modifications are the initial dominant influence of Nox4 ROS on the RyR1 although alternate modifications may subsequently occur that contribute to the overall leakiness of the channel. Future work utilising mass spectrometry and proteomics would aid in providing greater detail as to specific locations and modifications.

We observed an increase in RyR1 expression in the Nox4$^{-/-}$ mouse. In our hands, the increase in basal RyR1 is difficult to explain as RyR1 protein increases are not typically observed. One report has previously found an increase in RyR1 mRNA in a sepsis model in rats [83] although no protein analysis was performed to determine if the increased mRNA translated to increased protein. Muscle cells from a model of Central Core Rod disease have been found to have more RyR1 present in the central core rods themselves [84]. Probing of CD68 showed no changes, suggesting no immune cell infiltration or contribution to the overall increase in the RyR1 expression in Nox4$^{-/-}$. The lack of immune cell involvement would suggest that the increase in RyR1 expression in Nox4$^{-/-}$ is indeed occurring within the skeletal muscle alone, raising the question as to where the increased RyR1 channels are located. At this stage, the reason behind this increase is still undetermined.

We also examined Nox2 ROS and Nox4 ROS deficient muscle for changes in key Ca^{2+} handling proteins. STIM1S, CSQ1 and SERCA1 were all found not to be different from WT. This is suggestive that the different ROS species present are not influencing compensatory expression changes in the Ca^{2+} handling proteins. While the total protein levels have not changed there is still the possibility of changes in function of the proteins due to oxidation or post-translational modifications yet this has not been assessed here.

To date, many of the studies examining the effects of ROS in skeletal muscle focus on changes to the contractile function of the fibres. ROS can alter myofilament Ca^{2+} sensitivity in addition to altering SR Ca^{2+} release during excitation-contraction coupling [54,79,[85], [86], [87], [88]]. There is also data suggesting that ROS produced during contraction can also delay recovery from fatigue [54,89]. While it may seem that ROS produced during exercise has a negative impact due to changes in the muscle's ability to produce force, studies have suggested that ROS regulates an adaptive response (hormesis) in the muscle [67,68]. Cheng et al. [54] used pharmacological inhibitors to target ROS from Nox2, Nox4 and the mitochondria in order to examine effects on single fibre muscle fatigue. Interestingly, they found minimal changes with the use of Nox inhibitors in muscle performance and recovery. The authors suggest that using whole muscle for these measurements could yield more consistent results. We examined force production, time to fatigue and recovery from fatigue in Nox4$^{-/-}$ EDL muscles. When compared to an age-matched WT mouse, we found no difference in our experimental parameters. This finding indicates that Nox4 ROS does not have a role in contributing to fatigue via changes to myofilament Ca^{2+} sensitivity or alterations in SR Ca^{2+} release upon activation.

While Nox4 did not appear to have a role in altering the force-generating properties of skeletal muscle, the functional role of Nox4 still needed to be determined. The RyR1 is known to be susceptible to S-nitrosylation, yet the mechanism behind this modification has remained unclear. We report a modest increase in S-Nitrosylation of the RyR1 in muscle from p47$^{-/-}$ with no alteration in the RyR1 in muscle from p47$^{-/-}$/*mdx*. As the RyR1 SNO data is expressed as a ratio over total RyR present, the large increase in RyR present in the Nox4$^{-/-}$ could be contributed to the overall decrease in RyR1 SNO. However, when RyR1 SNO is expressed relative to MHC (for total protein), RyR1 SNO remains

significantly decreased. Future studies would examine the exact cysteine thiols that are nitrosylated in order to provide further insight, as our studies are looking at bulk nitrosylation of the RyR1. Nox2 and Nox4 produce superoxide and H_2O_2, which can lead to protein carbonylation; so how might Nox ROS promote S-Nitrosylation of RyR1? Hydrogen peroxide has been shown to promote NOS dependent NO production and subsequent protein S-Nitrosylation in endothelial cells (eNOS) [90], cardiomyocytes (nNOS) [91], and skeletal myotubes (nNOS) [92]. Furthermore, H_2O_2 has been show to activate nitrate reductase [[93], [94], [95]], an enzyme which catalyzes NAD(P)H-dependent reduction of nitrite to NO, and nitrate reductase generated NO has been shown to play a role in functional hyperemia in skeletal muscle [96]. Cellular nano-domains can respond quickly to Nox derived ROS, suggesting that Nox ROS may be exerting actions via affecting signaling targets close to the ROS source i.e. RyR1 proximity to Nox4. Thus, Nox4 derived H_2O_2 may promote protein carbonylation as well as increased NO production directly through increased NOS activity or through activation of nitrate reductase; with subsequent RyR1 S-Nitrosylation.

In Fig. 7, we propose a model of Ca^{2+} and ROS interplay in the triadic junctional space. This model has been generated based on the *mdx* mouse. Contrary to our initial hypothesis of t-tubular Nox2 ROS initiating RyR leak, we found Ca^{2+} leak persists in mouse models that cannot generate Nox2 ROS. The overall improvement in the phenotype of the $p47^{-/-}$/*mdx* mouse [13,50,51] suggests that perhaps Nox2 ROS production is exacerbated in the *mdx* mouse by the local increase of Ca^{2+} within the junctional space from the RyR1 leak. This reciprocal interplay between Ca^{2+} and ROS is consistent with previous findings in skeletal muscle and cardiac fibres [19,25,97].

Open in a separate window

Fig. 7

Model of the cascade of ROS/Ca^{2+}interactions that occur in the skeletal muscle triadic micro-domain.1. Nox4 ROS contributes to an increase in S-nitrosylation of the RyR1, resulting in increased Ca^{2+}leak from the RyR1 into the junctional space. 2. Increased Ca^{2+}in the junctional space due to the RyR1 Ca^{2+}leak promotes increased Nox2 ROS activation and production. 3. Increased Ca^{2+}influx from the extracellular space also contributes to Nox2 activation and ROS production. 4. Increased Ca^{2+}in the bulk cytoplasm and the junctional space, in addition to the increased Nox2 ROS leads to alterations in autophagy, protein degradation and other cellular functions which contributes to the pathology observed in dystrophic skeletal muscle.

In our model, we propose a multistep process of Ca^{2+} and ROS interactions within the triadic micro-domain. Initially, Nox4 ROS drives changes to the RyR1 via s-nitrosylation modifications leading to increased Ca^{2+} leak (step 1). The increase in Ca^{2+} leak promotes a higher $[Ca^{2+}]_{js}$ and promotes enhanced Nox2 activation and ROS production (step 2). During this time in the *mdx* mouse model, increased Ca^{2+} influx from the extracellular space is also contributing to the activation of Nox2 [[21], [27], [51]] (step 3). Increased Ca^{2+} in the bulk cytoplasm and junctional space as well as increased Nox2 ROS and potentially increased mitochondrial ROS leads to impairment of cellular functions such as autophagy [[98], [99], [100], [101]], ER stress [[102], [103], [104]], or mitochondrial Ca^{2+} accumulation [105] (step 4). As the steps in our model are occurring at rest in skeletal muscle, the alteration in calcium homeostasis and redox balance could also lead to changes in force production [88,106] or compensatory mechanisms. The disruption of these processes contributes to the pathology

observed in dystrophic muscle and potentially in many other disease types. The persistent RyR1 leak could also serve to induce mitochondrial biogenesis [81] which would also alter the muscles' capacity for performance and metabolism, driving compensatory mechanisms within the cell. These compensatory mechanisms could assist in allowing the cell to adapt, for example, during exercise, or push the cell to a pathological state. Recently it has been shown that Ca^{2+} from RyR1 leak can accumulate in the mitochondria [105]. In the model we propose here, the mitochondrial accumulation of Ca^{2+} would be occurring in the bulk cytoplasm, as a consequence of the events outlined in the triadic micro-domain.

As Nox4 is constitutively active but can be regulated in an inducible manner [107], for many cell types and situations, the precursor to alterations in Nox4 will need to be determined. Nox4 can serve as an inflammation promotion factor, with expression increasing as inflammatory markers such as Cox2, IL-1β and TNF-α are increased [108]. In vasculature cells, it appears that the circadian clock can influence Nox4 expression with alterations in the circadian rhythm, causing ROS production [109]. There are multiple transcription factors that can alter Nox4 promoter activity; such as NFκB, SMAD2/3, TGFβ, E2F, HIF1α and Nrf2 [110]. In dystrophic muscle, the persistent degeneration/regeneration cycles lead to increased TGFβ exposure and inflammatory cell infiltrate [111]. This increase in TGFβ could, in turn, lead to increased Nox4 expression and initiate the RyR1 leak seen in the *mdx* mouse.

5. Conclusion

Nox4 ROS induces RyR1 Ca^{2+} leak, via S-nitrosylation modifications. Although Nox2 ROS does not directly contribute to RyR1 leak, it responds reciprocally to the increased Ca^{2+} in the junctional space from the RyR1 leak and to the increased Ca^{2+} influx from the extracellular compartment. The reciprocal interplay between the Nox isoforms and Ca^{2+} occurs within the triad of skeletal muscle as the plasma membrane has been peeled back during the mechanical skinning process. Our model of the cascade of ROS and Ca^{2+} interactions highlights the importance of assessing these movements not only in skeletal muscle as a whole, but within and around organelle micro-domains.

Declaration of competing interest

None.

Acknowledgements

The authors would like to thank Courtney Carvasos for technical assistance. The monoclonal RyR1 antibody (34C) developed by J. Airey and J. Sutko and the SERCA antibody (CA F2-5D2) developed by Dr Fambrough, were obtained from the Developmental Studies Hybridoma Bank developed under the auspices of the NICHD, National Institutes of Health, and maintained by the University of Iowa (Iowa City, IA, USA).

Footnotes

Appendix A Supplementary data to this article can be found online at https://doi.org/10.1016/j.redox.2020.101557.

Funding sources

This work was supported by the National Institutes of Health (AR061370) and The Department of Defense (MD170090).

Appendix A. Supplementary data

The following are the Supplementary data to this article:

Multimedia component 1:

Click here to view.(244 bytes, xml)Multimedia component 1

References

1. Melzer W., Herrmann-Frank A., Luttgau H.C. The role of Ca2+ ions in excitation-contraction coupling of skeletal muscle fibres. *Biochim. Biophys. Acta.* 1995;1241:59–116. [PubMed] [Google Scholar]

2. Franzini-Armstrong C. The relationship between form and function throughout the history of excitation-contraction coupling. *J. Gen. Physiol.* 2018;150:189–210. doi: 10.1085/jgp.201711889. [PMC free article] [PubMed] [CrossRef] [Google Scholar]

3. Cully T.R. Junctional membrane Ca(2+) dynamics in human muscle fibers are altered by malignant hyperthermia causative RyR mutation. *Proc. Natl. Acad. Sci. U. S. A.* 2018;115:8215–8220. doi: 10.1073/pnas.1800490115. [PMC free article] [PubMed] [CrossRef] [Google Scholar]

4. Launikonis B.S., Cully T.R., Csernoch L., Stephenson D.G. NHE- and diffusion-dependent proton fluxes across the tubular system membranes of fast-twitch muscle fibers of the rat. *J. Gen. Physiol.* 2018;150:95–110. doi: 10.1085/jgp.201711891. [PMC free article] [PubMed] [CrossRef] [Google Scholar]

5. Murphy R.M. Ca2+-dependent proteolysis of junctophilin-1 and junctophilin-2 in skeletal and cardiac muscle. *J. Physiol.* 2013;591:719–729. doi: 10.1113/jphysiol.2012.243279. [PMC free article] [PubMed] [CrossRef] [Google Scholar]

6. Murphy R.M., Verburg E., Lamb G.D. Ca2+ activation of diffusible and bound pools of mu-calpain in rat skeletal muscle. *J. Physiol.* 2006;576:595–612. doi: 10.1113/jphysiol.2006. jphysiol.2006.114090 [pii] 114090. [PMC free article] [PubMed] [CrossRef] [Google Scholar]

7. Gailly P., De Backer F., Van Schoor M., Gillis J.M. In situ measurements of calpain activity in isolated muscle fibres from normal and dystrophin-lacking mdx mice. *J. Physiol.* 2007;582:1261–1275. doi: 10.1113/jphysiol.2007.132191. [PMC free article] [PubMed] [CrossRef] [Google Scholar]

8. Bedard K., Krause K.H. The NOX family of ROS-generating NADPH oxidases: physiology and pathophysiology. *Physiol. Rev.* 2007;87:245–313. doi: 10.1152/physrev.00044.2005. [PubMed] [CrossRef] [Google Scholar]

9. Sakellariou G.K., Jackson M.J., Vasilaki A. Redefining the major contributors to superoxide production in contracting skeletal muscle. The role of NAD(P)H oxidases. *Free Radic. Res.* 2014;48:12–29. doi: 10.3109/10715762.2013.830718. [PubMed] [CrossRef] [Google Scholar]

10. Sen C.K. Antioxidant and redox regulation of cellular signaling: introduction. *Med. Sci. Sports Exerc.* 2001;33:368–370. [PubMed] [Google Scholar]

11. Chen J.R. p47phox-Nox2-dependent ROS signaling inhibits early bone development in mice but protects against skeletal aging. *J. Biol. Chem.* 2015;290:14692–14704. doi: 10.1074/jbc.M114.633461. [PMC free article] [PubMed] [CrossRef] [Google Scholar]

12. Patel V.B. Loss of p47phox subunit enhances susceptibility to biomechanical stress and heart failure because of dysregulation of cortactin and actin filaments. *Circ. Res.* 2013;112:1542–1556. doi: 10.1161/CIRCRESAHA.111.300299. [PubMed] [CrossRef] [Google Scholar]

13. Pal R. Src-dependent impairment of autophagy by oxidative stress in a mouse model of Duchenne muscular dystrophy. *Nat. Commun.* 2014;5:4425. doi: 10.1038/ncomms5425. [PMC free article] [PubMed] [CrossRef] [Google Scholar]

14. Jackson S.H., Gallin J.I., Holland S.M. The p47phox mouse knock-out model of chronic granulomatous disease. *J. Exp. Med.* 1995;182:751–758. doi: 10.1084/jem.182.3.751. [PMC free article] [PubMed] [CrossRef] [Google Scholar]

15. Sun Q.A. Oxygen-coupled redox regulation of the skeletal muscle ryanodine receptor-Ca2+ release channel by NADPH oxidase 4. *Proc. Natl. Acad. Sci. U. S. A.* 2011;108:16098–16103. doi: 10.1073/pnas.1109546108. [PMC free article] [PubMed] [CrossRef] [Google Scholar]

16. Nisimoto Y., Diebold B.A., Cosentino-Gomes D., Lambeth J.D. Nox4: a hydrogen peroxide-generating oxygen sensor. *Biochemistry.* 2014;53:5111–5120. doi: 10.1021/bi500331y. [PMC free article] [PubMed] [CrossRef] [Google Scholar]

17. von Lohneysen K., Noack D., Jesaitis A.J., Dinauer M.C., Knaus U.G. Mutational analysis reveals distinct features of the Nox4-p22 phox complex. *J. Biol. Chem.* 2008;283:35273–35282. doi: 10.1074/jbc.M804200200. [PMC free article] [PubMed] [CrossRef] [Google Scholar]

18. Whitehead N.P., Yeung E.W., Froehner S.C., Allen D.G. Skeletal muscle NADPH oxidase is increased and triggers stretch-induced damage in the mdx mouse. *PloS One.* 2010;5 doi: 10.1371/journal.pone.0015354. [PMC free article] [PubMed] [CrossRef] [Google Scholar]

19. Shkryl V.M. Reciprocal amplification of ROS and Ca(2+) signals in stressed mdx dystrophic skeletal muscle fibers. *Pflügers Archiv.* 2009;458:915–928. doi: 10.1007/s00424-009-0670-2. [PubMed] [CrossRef] [Google Scholar]

20. Hidalgo C., Sanchez G., Barrientos G., Aracena-Parks P. A transverse tubule NADPH oxidase activity stimulates calcium release from isolated triads via ryanodine receptor type 1 S -glutathionylation. *J. Biol. Chem.* 2006;281:26473–26482. doi: 10.1074/jbc.M600451200. M600451200 [pii] [PubMed] [CrossRef] [Google Scholar]

21. Turner P.R., Fong P.Y., Denetclaw W.F., Steinhardt R.A. Increased calcium influx in dystrophic muscle. *J. Cell Biol.* 1991;115:1701–1712. [PMC free article] [PubMed] [Google Scholar]

22. Head S.I. Branched fibres in old dystrophic mdx muscle are associated with mechanical weakening of the sarcolemma, abnormal Ca2+ transients and a breakdown of Ca2+ homeostasis during fatigue. *Exp. Physiol.* 2010;95:641–656. doi: 10.1113/expphysiol.2009. expphysiol.2009.052019 [pii] 052019. [PubMed] [CrossRef] [Google Scholar]

23. Yeung E.W. Effects of stretch-activated channel blockers on [Ca2+]i and muscle damage in the mdx mouse. *J. Physiol.* 2005;562:367–380. doi: 10.1113/jphysiol.2004.075275. [PMC free article] [PubMed] [CrossRef] [Google Scholar]

24. Burr A.R., Molkentin J.D. Genetic evidence in the mouse solidifies the calcium hypothesis of myofiber death in muscular dystrophy. *Cell Death Differ.* 2015;22:1402–1412. doi: 10.1038/cdd.2015.65. [PMC free article] [PubMed] [CrossRef] [Google Scholar]

25. Whitehead N.P., Yeung E.W., Allen D.G. Muscle damage in mdx (dystrophic) mice: role of calcium and reactive oxygen species. *Clin. Exp. Pharmacol. Physiol.* 2006;33:657–662. doi: 10.1111/j.1440-1681.2006.04394.x. CEP [pii] [PubMed] [CrossRef] [Google Scholar]

26. Gillis J.M. Understanding dystrophinopathies: an inventory of the structural and functional consequences of the absence of dystrophin in muscles of the mdx mouse. *J. Muscle Res. Cell Motil.* 1999;20:605–625. [PubMed] [Google Scholar]

27. Edwards J.N. Upregulation of store-operated Ca2+ entry in dystrophic mdx mouse muscle. *Am. J. Physiol. Cell Physiol.* 2010;299:C42–C50. doi: 10.1152/ajpcell.00524. ajpcell.00524.2009 [pii] 2009. [PubMed] [CrossRef] [Google Scholar]

28. Whitehead N.P., Pham C., Gervasio O.L., Allen D.G. N-Acetylcysteine ameliorates skeletal muscle pathophysiology in mdx mice. *J. Physiol.* 2008;586:2003–2014. doi: 10.1113/jphysiol.2007. jphysiol.2007.148338 [pii] 148338. [PMC free article] [PubMed] [CrossRef] [Google Scholar]

29. Whitehead, N. P., Yeung, E. W., Froehner, S. C. & Allen, D. G. Skeletal muscle NADPH oxidase is increased and triggers stretch-induced damage in the mdx mouse. PloS One 5, e15354, doi:10.1371/journal.pone.0015354. [PMC free article] [PubMed]

30. Cully T.R., Launikonis B.S. Leaky ryanodine receptors delay the activation of store overload-induced Ca2+ release, a mechanism underlying malignant hyperthermia-like events in dystrophic muscle. *Am. J. Physiol. Cell Physiol.* 2016;310:C673–C680. doi: 10.1152/ajpcell.00366.2015. [PubMed] [CrossRef] [Google Scholar]

31. Bellinger A.M. Hypernitrosylated ryanodine receptor calcium release channels are leaky in dystrophic muscle. *Nat. Med.* 2009;15:325–330. doi: 10.1038/nm.1916. [PMC free article] [PubMed] [CrossRef] [Google Scholar]

32. Cully T.R., Launikonis B.S. Assessment of RyR leak and t-system Ca2+ uptake in dystrophic skeletal muscle. *Proc Aust Physiol Soc.* 2014;46:85p. [Google Scholar]

33. Carnesecchi S. A key role for NOX4 in epithelial cell death during development of lung fibrosis. *Antioxidants Redox Signal.* 2011;15:607–619. doi: 10.1089/ars.2010.3829. [PMC free article] [PubMed] [CrossRef] [Google Scholar]

34. Kadoguchi T. Possible role of NADPH oxidase 4 in angiotensin II-induced muscle wasting in mice. *Front. Physiol.* 2018;9:340. doi: 10.3389/fphys.2018.00340. [PMC free article] [PubMed] [CrossRef] [Google Scholar]

35. Lamb G.D., Junankar P.R., Stephenson D.G. Raised intracellular [Ca2+] abolishes excitation-contraction coupling in skeletal muscle fibres of rat and toad. *J. Physiol.* 1995;489(Pt 2):349–362. [PMC free article] [PubMed] [Google Scholar]

36. Lamb G.D., Stephenson D.G. Control of calcium release and the effect of ryanodine in skinned muscle fibres of the toad. *J. Physiol.* 1990;423:519–542. [PMC free article] [PubMed] [Google Scholar]

37. Lamb G.D., Stephenson D.G. Effects of intracellular pH and [Mg2+] on excitation-contraction coupling in skeletal muscle fibres of the rat. *J. Physiol.* 1994;478(Pt 2):331–339. [PMC free article] [PubMed] [Google Scholar]

38. Cully T.R., Edwards J.N., Murphy R.M., Launikonis B.S. A quantitative description of tubular system Ca(2+) handling in fast- and slow-twitch muscle fibres. *J. Physiol.* 2016;594:2795–2810. doi: 10.1113/JP271658. [PMC free article] [PubMed] [CrossRef] [Google Scholar]

39. Cully T.R. Human skeletal muscle plasmalemma alters its structure to change its Ca2+-handling following heavy-load resistance exercise. *Nat. Commun.* 2017;8:14266. doi: 10.1038/ncomms14266. [PMC free article] [PubMed] [CrossRef] [Google Scholar]

40. Mollica J.P., Oakhill J.S., Lamb G.D., Murphy R.M. Are genuine changes in protein expression being overlooked? Reassessing Western blotting. *Anal. Biochem.* 2009;386:270–275. doi: 10.1016/j.ab.2008.12.029. S0003-2697(08)00853-1 [pii] [PubMed] [CrossRef] [Google Scholar]

41. Murphy R.M., Lamb G.D. Important considerations for protein analyses using antibody based techniques: down-sizing Western blotting up-sizes outcomes. *J. Physiol.* 2013;591:5823–5831. doi: 10.1113/jphysiol.2013.263251. [PMC free article] [PubMed] [CrossRef] [Google Scholar]

42. Murphy R.M., Mollica J.P., Beard N.A., Knollmann B.C., Lamb G.D. Quantification of calsequestrin 2 (CSQ2) in sheep cardiac muscle and Ca2+-binding protein changes in CSQ2 knockout mice. *Am. J. Physiol. Heart Circ. Physiol.* 2011;300:H595–H604. doi: 10.1152/ajpheart.00902.2010. [PMC free article] [PubMed] [CrossRef] [Google Scholar]

43. Murphy R.M. Activation of skeletal muscle calpain-3 by eccentric exercise in humans does not result in its translocation to the nucleus or cytosol. *J. Appl. Physiol.* 1985;111:1448–1458. doi: 10.1152/japplphysiol.00441.2011. 2011. [PubMed] [CrossRef] [Google Scholar]

44. Murphy R.M. Enhanced technique to measure proteins in single segments of human skeletal muscle fibers: fiber-type dependence of AMPK-alpha1 and -beta1. *J. Appl. Physiol.* 2011;110:820–825. doi: 10.1152/japplphysiol.01082. japplphysiol.01082.2010 [pii] 2010. [PubMed] [CrossRef] [Google Scholar]

45. Fortes M.A. Housekeeping proteins: how useful are they in skeletal muscle diabetes studies and muscle hypertrophy models? *Anal. Biochem.* 2016;504:38–40. doi: 10.1016/j.ab.2016.03.023. [PubMed] [CrossRef] [Google Scholar]

46. Lowe D.A., Degens H., Chen K.D., Alway S.E. Glyceraldehyde-3-phosphate dehydrogenase varies with age in glycolytic muscles of rats. *J Gerontol A Biol Sci Med Sci.* 2000;55:B160–B164. doi: 10.1093/gerona/55.3.b160. [PubMed] [CrossRef] [Google Scholar]

47. Vigelso A. GAPDH and beta-actin protein decreases with aging, making Stain-Free technology a superior loading control in Western blotting of human skeletal muscle. *J. Appl. Physiol.* 2015;118:386–394. doi: 10.1152/japplphysiol.00840.2014. [PubMed] [CrossRef] [Google Scholar]

48. Rivero-Gutierrez B., Anzola A., Martinez-Augustin O., de Medina F.S. Stain-free detection as loading control alternative to Ponceau and housekeeping protein immunodetection in Western blotting. *Anal. Biochem.* 2014;467:1–3. doi: 10.1016/j.ab.2014.08.027. [PubMed] [CrossRef] [Google Scholar]

49. Colella A.D. Comparison of Stain-Free gels with traditional immunoblot loading control methodology. *Anal. Biochem.* 2012;430:108–110. doi: 10.1016/j.ab.2012.08.015. [PubMed] [CrossRef] [Google Scholar]

50. Loehr J.A. NADPH oxidase mediates microtubule alterations and diaphragm dysfunction in dystrophic mice. *Elife.* 2018;7 doi: 10.7554/eLife.31732. [PMC free article] [PubMed] [CrossRef] [Google Scholar]

51. Loehr J.A. Eliminating Nox2 reactive oxygen species production protects dystrophic skeletal muscle from pathological calcium influx assessed in vivo by manganese-enhanced magnetic resonance imaging. *J. Physiol.* 2016;594:6395–6405. doi: 10.1113/JP272907. [PMC free article] [PubMed] [CrossRef] [Google Scholar]

52. Zana M. Interaction between p22(phox) and Nox4 in the endoplasmic reticulum suggests a unique mechanism of NADPH oxidase complex formation. *Free Radic. Biol. Med.* 2018;116:41–49. doi: 10.1016/j.freeradbiomed.2017.12.031. [PubMed] [CrossRef] [Google Scholar]

53. Zhang M., Perino A., Ghigo A., Hirsch E., Shah A.M. NADPH oxidases in heart failure: poachers or gamekeepers? *Antioxidants Redox Signal.* 2013;18:1024–1041. doi: 10.1089/ars.2012.4550. [PMC free article] [PubMed] [CrossRef] [Google Scholar]

54. Cheng A.J., Bruton J.D., Lanner J.T., Westerblad H. Antioxidant treatments do not improve force recovery after fatiguing stimulation of mouse skeletal muscle fibres. *J. Physiol.* 2015;593:457–472. doi: 10.1113/jphysiol.2014.279398. [PMC free article] [PubMed] [CrossRef] [Google Scholar]

55. Edwards J.N. Ultra-rapid activation and deactivation of store-operated Ca(2+) entry in skeletal muscle. *Cell Calcium.* 2010;47:458–467. doi: 10.1016/j.ceca.2010.04.001. [PubMed] [CrossRef] [Google Scholar]

56. Cully T.R., Friedrich O., Edwards J.N., Murphy R.M., Launikonis B.S. Store-dependent Ca^{2+} influx in intact healthy and dystrophic skeletal muscle. *Proc Aust Physiol Soc.* 2008;39:78P. [Google Scholar]

57. Cully T.R., Launikonis B.S. Store-operated Ca(2)(+) entry is not required for store refilling in skeletal muscle. *Clin. Exp. Pharmacol. Physiol.* 2013;40:338–344. doi: 10.1111/1440-1681.12078. [PubMed] [CrossRef] [Google Scholar]

58. Lewis R.S. The molecular choreography of a store-operated calcium channel. *Nature.* 2007;446:284–287. doi: 10.1038/nature05637. nature05637 [pii] [PubMed] [CrossRef] [Google Scholar]

59. Darbellay B., Arnaudeau S., Bader C.R., Konig S., Bernheim L. STIM1L is a new actin-binding splice variant involved in fast repetitive Ca2+ release. *J. Cell Biol.* 2011;194:335–346. doi: 10.1083/jcb.201012157. jcb.201012157 [pii] [PMC free article] [PubMed] [CrossRef] [Google Scholar]

60. Cully T.R. Changes in plasma membrane Ca-ATPase and stromal interacting molecule 1 expression levels for Ca(2+) signaling in dystrophic mdx mouse muscle. *Am. J. Physiol. Cell Physiol.* 2012;303:C567–C576. doi: 10.1152/ajpcell.00144.2012. [PubMed] [CrossRef] [Google Scholar]

61. Hosoi E. Expression of the ryanodine receptor isoforms in immune cells. *J. Immunol.* 2001;167:4887–4894. [PubMed] [Google Scholar]

62. Reiken S. PKA phosphorylation activates the calcium release channel (ryanodine receptor) in skeletal muscle: defective regulation in heart failure. *J. Cell Biol.* 2003;160:919–928. doi: 10.1083/jcb.200211012. [PMC free article] [PubMed] [CrossRef] [Google Scholar]

63. Berridge M.J., Bootman M.D., Roderick H.L. Calcium signalling: dynamics, homeostasis and remodelling. *Nat. Rev. Mol. Cell Biol.* 2003;4:517–529. doi: 10.1038/nrm1155nrm1155. [pii] [PubMed] [CrossRef] [Google Scholar]

64. Yeung E.W., Balnave C.D., Ballard H.J., Bourreau J.P., Allen D.G. Development of T-tubular vacuoles in eccentrically damaged mouse muscle fibres. *J. Physiol.* 2002;540:581–592. [PMC free article] [PubMed] [Google Scholar]

65. Yeung E.W., Allen D.G. Stretch-activated channels in stretch-induced muscle damage: role in muscular dystrophy. *Clin. Exp. Pharmacol. Physiol.* 2004;31:551–556. doi: 10.1111/j.1440-1681.2004.04027.x. [PubMed] [CrossRef] [Google Scholar]

66. Reid M.B. Invited Review: redox modulation of skeletal muscle contraction: what we know and what we don't. *J. Appl. Physiol.* 2001;90:724–731. [PubMed] [Google Scholar]

67. Radak Z. Exercise, oxidants, and antioxidants change the shape of the bell-shaped hormesis curve. *Redox Biol.* 2017;12:285–290. doi: 10.1016/j.redox.2017.02.015. [PMC free article] [PubMed] [CrossRef] [Google Scholar]

68. Hancock M. Myocardial NADPH oxidase-4 regulates the physiological response to acute exercise. *Elife.* 2018;7 doi: 10.7554/eLife.41044. [PMC free article] [PubMed] [CrossRef] [Google Scholar]

69. Pal R., Basu Thakur P., Li S., Minard C., Rodney G.G. Real-time imaging of NADPH oxidase activity in living cells using a novel fluorescent protein reporter. *PloS One.* 2013;8 doi: 10.1371/journal.pone.0063989. [PMC free article] [PubMed] [CrossRef] [Google Scholar]

70. Kalyanaraman B. Measuring reactive oxygen and nitrogen species with fluorescent probes: challenges and limitations. *Free Radic. Biol. Med.* 2012;52:1–6. doi: 10.1016/j.freeradbiomed.2011.09.030. [PMC free article] [PubMed] [CrossRef] [Google Scholar]

71. Gibhardt C.S., Zimmermann K.M., Zhang X., Belousov V.V., Bogeski I. Imaging calcium and redox signals using genetically encoded fluorescent indicators. *Cell Calcium.* 2016;60:55–64. doi: 10.1016/j.ceca.2016.04.008. [PubMed] [CrossRef] [Google Scholar]

72. Prior K.K. CRISPR/Cas9-mediated knockout of p22phox leads to loss of Nox1 and Nox4, but not Nox5 activity. *Redox Biol.* 2016;9:287–295. doi: 10.1016/j.redox.2016.08.013. [PMC free article] [PubMed] [CrossRef] [Google Scholar]

73. Durham W.J. RyR1 S-nitrosylation underlies environmental heat stroke and sudden death in Y522S RyR1 knockin mice. *Cell.* 2008;133:53–65. doi: 10.1016/j.cell.2008.02.042. [PMC free article] [PubMed] [CrossRef] [Google Scholar]

74. Lanner J.T., Georgiou D.K., Joshi A.D., Hamilton S.L. Ryanodine receptors: structure, expression, molecular details, and function in calcium release. *Cold Spring Harb Perspect Biol.* 2010;2:a003996. doi: 10.1101/cshperspect.a003996. [PMC free article] [PubMed] [CrossRef] [Google Scholar]

75. Aracena P., Tang W., Hamilton S.L., Hidalgo C. Effects of S-glutathionylation and S-nitrosylation on calmodulin binding to triads and FKBP12 binding to type 1 calcium release channels. *Antioxidants Redox Signal.* 2005;7:870–881. doi: 10.1089/ars.2005.7.870. [PubMed] [CrossRef] [Google Scholar]

76. Aracena-Parks P. Identification of cysteines involved in S-nitrosylation, S-glutathionylation, and oxidation to disulfides in ryanodine receptor type 1. *J. Biol. Chem.* 2006;281:40354–40368. doi: 10.1074/jbc.M600876200. [PubMed] [CrossRef] [Google Scholar]

77. Lamboley C.R. Contractile properties and sarcoplasmic reticulum calcium content in type I and type II skeletal muscle fibres in active aged humans. *J. Physiol.* 2015;593:2499–2514. doi: 10.1113/JP270179. [PMC free article] [PubMed] [CrossRef] [Google Scholar]

78. Voss A.A., Lango J., Ernst-Russell M., Morin D., Pessah I.N. Identification of hyperreactive cysteines within ryanodine receptor type 1 by mass spectrometry. *J. Biol. Chem.* 2004;279:34514–34520. doi: 10.1074/jbc.M404290200. [PubMed] [CrossRef] [Google Scholar]

79. Dutka T.L. S-nitrosylation and S-glutathionylation of Cys134 on troponin I have opposing competitive actions on Ca(2+) sensitivity in rat fast-twitch muscle fibers. *Am. J. Physiol. Cell Physiol.* 2017;312:C316–C327. doi: 10.1152/ajpcell.00334.2016. [PubMed] [CrossRef] [Google Scholar]

80. Marx S.O. PKA phosphorylation dissociates FKBP12.6 from the calcium release channel (ryanodine receptor): defective regulation in failing hearts. *Cell.* 2000;101:365–376. doi: 10.1016/s0092-8674(00)80847-8. [PubMed] [CrossRef] [Google Scholar]

81. Ivarsson N. SR Ca(2+) leak in skeletal muscle fibers acts as an intracellular signal to increase fatigue resistance. *J. Gen. Physiol.* 2019;151:567–577. doi: 10.1085/jgp.201812152. [PMC free article] [PubMed] [CrossRef] [Google Scholar]

82. Aydin J. Nonshivering thermogenesis protects against defective calcium handling in muscle. *Faseb. J.* 2008;22:3919–3924. doi: 10.1096/fj.08-113712. fj.08-113712 [pii] [PMC free article] [PubMed] [CrossRef] [Google Scholar]

83. Rossignol B. Effects of chronic sepsis on contractile properties of fast twitch muscle in an experimental model of critical illness neuromyopathy in the rat. *Crit. Care Med.* 2008;36:1855–1863. doi: 10.1097/CCM.0b013e318176106b. [PubMed] [CrossRef] [Google Scholar]

84. Scacheri P.C. A novel ryanodine receptor gene mutation causing both cores and rods in congenital myopathy. *Neurology.* 2000;55:1689–1696. doi: 10.1212/wnl.55.11.1689. [PubMed] [CrossRef] [Google Scholar]

85. Westerblad H., Allen D.G. Changes of myoplasmic calcium concentration during fatigue in single mouse muscle fibers. *J. Gen. Physiol.* 1991;98:615–635. [PMC free article] [PubMed] [Google Scholar]

86. Lamboley C.R., Wyckelsma V.L., McKenna M.J., Murphy R.M., Lamb G.D. Ca(2+) leakage out of the sarcoplasmic reticulum is increased in type I skeletal muscle fibres in aged humans. *J. Physiol.* 2016;594:469–481. doi: 10.1113/JP271382. [PMC free article] [PubMed] [CrossRef] [Google Scholar]

87. Andrade F.H., Reid M.B., Allen D.G., Westerblad H. Effect of hydrogen peroxide and dithiothreitol on contractile function of single skeletal muscle fibres from the mouse. *J. Physiol.* 1998;509(Pt 2):565–575. [PMC free article] [PubMed] [Google Scholar]

88. Lamb G.D., Posterino G.S. Effects of oxidation and reduction on contractile function in skeletal muscle fibres of the rat. *J. Physiol.* 2003;546:149–163. [PMC free article] [PubMed] [Google Scholar]

89. Lannergren J., Westerblad H., Bruton J.D. Slow recovery of force in single skeletal muscle fibres. *Acta Physiol. Scand.* 1996;156:193–202. [PubMed] [Google Scholar]

90. Thomas S., Kotamraju S., Zielonka J., Harder D.R., Kalyanaraman B. Hydrogen peroxide induces nitric oxide and proteosome activity in endothelial cells: a bell-shaped signaling response. *Free Radic. Biol. Med.* 2007;42:1049–1061. doi: 10.1016/j.freeradbiomed.2007.01.005. [PMC free article] [PubMed] [CrossRef] [Google Scholar]

91. Kar R., Kellogg D.L., Iii, Roman L.J. Oxidative stress induces phosphorylation of neuronal NOS in cardiomyocytes through AMP-activated protein kinase (AMPK) *Biochem. Biophys. Res. Commun.* 2015;459:393–397. doi: 10.1016/j.bbrc.2015.02.113. [PMC free article] [PubMed] [CrossRef] [Google Scholar]

92. Kellogg D.L., 3rd, McCammon K.M., Hinchee-Rodriguez K.S., Adamo M.L., Roman L.J. Neuronal nitric oxide synthase mediates insulin- and oxidative stress-induced glucose uptake in skeletal muscle myotubes. *Free Radic. Biol. Med.* 2017;110:261–269. doi: 10.1016/j.freeradbiomed.2017.06.018. [PMC free article] [PubMed] [CrossRef] [Google Scholar]

93. Lin A. Nitric oxide and protein S-nitrosylation are integral to hydrogen peroxide-induced leaf cell death in rice. *Plant Physiol.* 2012;158:451–464. doi: 10.1104/pp.111.184531. [PMC free article] [PubMed] [CrossRef] [Google Scholar]

94. Desikan R., Griffiths R., Hancock J., Neill S. A new role for an old enzyme: nitrate reductase-mediated nitric oxide generation is required for abscisic acid-induced stomatal closure in Arabidopsis thaliana. *Proc. Natl. Acad. Sci. U. S. A.* 2002;99:16314–16318. doi: 10.1073/pnas.252461999. [PMC free article] [PubMed] [CrossRef] [Google Scholar]

95. Kenis J.D., Morlans J.D., Trippi V.S. Effect of hydrogen peroxide on nitrate reductase activity in detached oat leaves in darkness. *Physiol. Plantarum.* 1989;76:216–220. doi: 10.1111/j.1399-3054.1989.tb05635.x. [CrossRef] [Google Scholar]

96. Piknova B., Park J.W., Kwan Jeff Lam K., Schechter A.N. Nitrate as a source of nitrite and nitric oxide during exercise hyperemia in rat skeletal muscle. *Nitric Oxide.* 2016;55–56:54–61. doi: 10.1016/j.niox.2016.03.005. [PMC free article] [PubMed] [CrossRef] [Google Scholar]

97. Wang Q., Wang W., Wang G., Rodney G.G., Wehrens X.H. Crosstalk between RyR2 oxidation and phosphorylation contributes to cardiac dysfunction in mice with Duchenne muscular dystrophy. *J. Mol. Cell. Cardiol.* 2015;89:177–184. doi: 10.1016/j.yjmcc.2015.11.009. [PMC free article] [PubMed] [CrossRef] [Google Scholar]

98. Filomeni G., De Zio D., Cecconi F. Oxidative stress and autophagy: the clash between damage and metabolic needs. *Cell Death Differ.* 2015;22:377–388. doi: 10.1038/cdd.2014.150. [PMC free article] [PubMed] [CrossRef] [Google Scholar]

99. Forte M., Palmerio S., Yee D., Frati G., Sciarretta S. Functional role of Nox4 in autophagy. *Adv. Exp. Med. Biol.* 2017;982:307–326. doi: 10.1007/978-3-319-55330-6_16. [PubMed] [CrossRef] [Google Scholar]

100. Kaminskyy V.O., Zhivotovsky B. Free radicals in cross talk between autophagy and apoptosis. *Antioxidants Redox Signal.* 2014;21:86–102. doi: 10.1089/ars.2013.5746. [PubMed] [CrossRef] [Google Scholar]

101. Rodney G.G., Pal R., Abo-Zahrah R. Redox regulation of autophagy in skeletal muscle. *Free Radic. Biol. Med.* 2016;98:103–112. doi: 10.1016/j.freeradbiomed.2016.05.010. [PMC free article] [PubMed] [CrossRef] [Google Scholar]

102. Pauly M. ER stress disturbs SR/ER-mitochondria Ca(2+) transfer: implications in Duchenne muscular dystrophy. *Biochim. Biophys. Acta (BBA) - Mol. Basis Dis.* 2017;1863:2229–2239. doi: 10.1016/j.bbadis.2017.06.009. [PubMed] [CrossRef] [Google Scholar]

103. Ersoy B.A., Maner-Smith K.M., Li Y., Alpertunga I., Cohen D.E. Thioesterase-mediated control of cellular calcium homeostasis enables hepatic ER stress. *J. Clin. Invest.* 2018;128:141–156. doi: 10.1172/JCI93123. [PMC free article] [PubMed] [CrossRef] [Google Scholar]

104. Kaufman R.J., Malhotra J.D. Calcium trafficking integrates endoplasmic reticulum function with mitochondrial bioenergetics. *Biochim. Biophys. Acta.* 2014;1843:2233–2239. doi: 10.1016/j.bbamcr.2014.03.022. [PMC free article] [PubMed] [CrossRef] [Google Scholar]

105. Canato M. Excessive accumulation of Ca2 + in mitochondria of Y522S-RYR1 knock-in mice: a link between leak from the sarcoplasmic reticulum and altered redox state. *Front. Physiol.* 2019;10 doi: 10.3389/fphys.2019.01142. [PMC free article] [PubMed] [CrossRef] [Google Scholar]

106. Andrade F.H., Reid M.B., Allen D.G., Westerblad H. Effect of nitric oxide on single skeletal muscle fibres from the mouse. *J. Physiol.* 1998;509(Pt 2):577–586. [PMC free article] [PubMed] [Google Scholar]

107. Shanmugasundaram K. NOX4 functions as a mitochondrial energetic sensor coupling cancer metabolic reprogramming to drug resistance. *Nat. Commun.* 2017;8:997. doi: 10.1038/s41467-017-01106-1. [PMC free article] [PubMed] [CrossRef] [Google Scholar]

108. Im Y.B. Molecular targeting of NOX4 for neuropathic pain after traumatic injury of the spinal cord. *Cell Death Dis.* 2012;3:e426. doi: 10.1038/cddis.2012.168. [PMC free article] [PubMed] [CrossRef] [Google Scholar]

109. Anea C.B. Circadian clock control of Nox4 and reactive oxygen species in the vasculature. *PloS One.* 2013;8 doi: 10.1371/journal.pone.0078626. [PMC free article] [PubMed] [CrossRef] [Google Scholar]

110. Chen F., Haigh S., Barman S., Fulton D. From form to function: the role of Nox4 in the cardiovascular system. *Front. Physiol.* 2012;3 doi: 10.3389/fphys.2012.00412. [PMC free article] [PubMed] [CrossRef] [Google Scholar]

111. Chen J.L., Colgan T.D., Walton K.L., Gregorevic P., Harrison C.A. The TGF-beta signalling network in muscle development, adaptation and disease. *Adv. Exp. Med. Biol.* 2016:97–131. doi: 10.1007/978-3-319-27511-6_5. 900. [PubMed] [CrossRef] [Google Scholar]